AJNR

Can Proton MR Spectroscopic and Perfusion Imaging Differentiate Between Neoplastic and Nonneoplastic Brain Lesions in Adults?

R. Hourani, L.J. Brant, T. Rizk, J.D. Weingart, P.B. Barker and A. Horská

AJNR Am J Neuroradiol 2008, 29 (2) 366-372
doi: https://doi.org/10.3174/ajnr.A0810
http://www.ajnr.org/content/29/2/366

ORIGINAL RESEARCH

Can Proton MR Spectroscopic and Perfusion Imaging Differentiate Between Neoplastic and Nonneoplastic Brain Lesions in Adults?

R. Hourani
L.J. Brant
T. Rizk
J.D. Weingart
P.B. Barker
A. Horská

BACKGROUND AND PURPOSE: Noninvasive diagnosis of brain lesions is important for the correct choice of treatment. Our aims were to investigate whether 1) proton MR spectroscopic imaging (^{1}H-MRSI) can aid in differentiating between tumors and nonneoplastic brain lesions, and 2) perfusion MR imaging can improve the classification.

MATERIALS AND METHODS: We retrospectively examined 69 adults with untreated primary brain lesions (brain tumors, $n = 36$; benign lesions, $n = 10$; stroke, $n = 4$; demyelination, $n = 10$; and stable lesions not confirmed on pathologic examination, $n = 9$). MR imaging and ^{1}H-MRSI were performed at 1.5T before biopsy or treatment. Concentrations of *N*-acetylaspartate (NAA), creatine (Cr), and choline (Cho) in the lesion were expressed as metabolite ratios and were normalized to the contralateral hemisphere. Dynamic susceptibility contrast-enhanced perfusion MR imaging was performed in a subset of patients ($n = 32$); relative cerebral blood volume (rCBV) was evaluated. Discriminant function analysis was used to identify variables that can predict inclusion in the neoplastic or nonneoplastic lesion groups. Receiver operator characteristic (ROC) analysis was used to compare the discriminatory capability of ^{1}H-MRSI and perfusion MR imaging.

RESULTS: The discriminant function analysis correctly classified 84.2% of original grouped cases ($P < .0001$), on the basis of NAA/Cho, Cho_{norm}, NAA_{norm}, and NAA/Cr ratios. MRSI and perfusion MR imaging had similar discriminatory capabilities in differentiating tumors from nonneoplastic lesions. With cutoff points of NAA/Cho $\leq$0.61 and rCBV $\geq$1.50 (corresponding to diagnosis of the tumors), a sensitivity of 72.2% and specificity of 91.7% in differentiating tumors from nonneoplastic lesions were achieved.

CONCLUSION: These results suggest a promising role for ^{1}H-MRSI and perfusion MR imaging in the distinction between brain tumors and nonneoplastic lesions in adults.

Noninvasive and accurate differentiation between neoplastic and nonneoplastic brain lesions is important in determining the correct treatment plan and, in some cases, may avoid the necessity of performing a biopsy.[1] Conventional structural MR imaging is an established and useful tool in the diagnosis and evaluation of brain tumors; however, it does not provide information on tumoral vascularity, metabolism, and cellularity, which are important in grading the tumor, and has a relatively low specificity for diagnosing mass lesions.[2] In many instances, reliable differentiation of neoplastic from nonneoplastic brain masses, or high-grade from low-grade tumors, is difficult or impossible with conventional MR imaging. As a result, some patients with benign lesions may undergo brain biopsies to rule out a neoplasm, an invasive procedure with an appreciable risk for morbidity.

Received March 22, 2007; accepted after revision July 29.

From the Russell H. Morgan Department of Radiology and Radiological Science (R.H., P.B.B., A.H.), and the Department of Neurological Surgery (J.D.W.), Johns Hopkins Hospital, Baltimore, Md; National Institutes of Health/National Institute on Aging, Gerontology Research Center (L.J.B.), Baltimore, Md; Department of Radiology (R.H.), American University of Beirut Medical Center, Beirut, Lebanon; Department of Neurosurgery (T.R.), Hotel Dieu Hospital, Beirut, Lebanon; and the FM Kirby Research Center (P.B.B.), Kennedy Krieger Institute, Baltimore, Md.

This publication was supported by NIH grant 1RO1 NS042851 and grant number P41 RR 015241 from the National Center for Research Resources (NCRR), a component of the National Institutes of Health (NIH). Its contents are solely the responsibility of the authors and do not necessarily represent the official view of NCRR or NIH.

Please address correspondence to Alena Horská, PhD, Russell H. Morgan Department of Radiology and Radiological Science, Johns Hopkins University, 217 Traylor Bldg, 720 Rutland Ave, Baltimore, MD 21205. E-mail: ahorska@jhmi.edu

DOI 10.3174/ajnr.A0810

Several types of nonneoplastic brain lesions (in particular, demyelinating lesions and lesions caused by infectious diseases) can be potentially misdiagnosed as brain tumors. The conventional MR imaging appearance of these lesions can be nonspecific, and even the use of a contrast agent is of limited benefit because any pathologic process associated with disruption of the blood-brain barrier can result in enhancement on MR imaging. Thus, there is a need for additional imaging modalities, such as MR spectroscopy and perfusion MR imaging, which may aid in improving the diagnosis of unknown brain lesions.[3] However, limited data are available on the use of proton MR spectroscopy (^{1}H-MRS) and perfusion MR imaging in the differentiation of nonneoplastic lesions from tumors. Although most of the previous studies used single-voxel spectroscopy with a relatively large voxel size, resulting in partial volume effects, they have indicated the promise of ^{1}H-MRS to differentiate between tumors and nonneoplastic lesions and adding diagnostic information.[1,4-7] Several groups also compared spectroscopic characteristics of specific groups of neoplastic and nonneoplastic lesions.[8-11] Two recent studies using perfusion MR imaging[12] and a combination of MR spectroscopic imaging (MRSI) and perfusion MR imaging[13] reported individual cases of lesions rather than group comparisons. Recently, multivoxel ^{1}H-MRSI differentiated 78% of originally grouped cases of nonneoplastic lesions and tumors in children.[14] We hypothesized that ^{1}H-MRSI can differentiate between brain tumors and nonneoplastic lesions in adults and that perfusion can further improve the

differentiation. High-resolution ^{1}H-MRSI allowed for evaluation of metabolite levels and corresponding blood volume in the regions of the lesions showing the most pronounced metabolic impairment.

Materials and Methods

We retrospectively examined 69 patients with primary brain lesions (mean age, 45.6 ± 13.1 years; age range, 20–77 years; 35 men). Patients were eligible for the study if they had a new, untreated primary brain lesion suspicious for a neoplasm on conventional MR imaging or CT scan. All patients were previously untreated, except for 3 cases of radiation necrosis in which the patients had had surgical treatment before with resection of extra-axial tumors (1 meningioma,1 chordoma, and 1 pituitary adenoma) and received radiation treatment; 1 case of a patient with acute myeloid leukemia treated with chemotherapy with secondary abnormal signal intensity in the brain that had remained stable for 3 years (at the time of the MRSI and perfusion scan); and 2 cases of patients with postsurgical gliosis that had been stable for 2.5 and 9 years. Forty-one patients subsequently underwent invasive diagnostic or surgical procedures (32 surgical procedures, 9 biopsies).

Thirty-six patients (mean age, 42.4 ± 15.3 years; 18 men) had brain tumors confirmed on neuropathologic examination (high-grade tumors, $n = 28$; low-grade tumors, $n = 8$), which were graded according to the World Health Organization (WHO) classification scheme. The diagnoses in the group of high-grade tumors included glioblastoma multiforme ($n = 13$), anaplastic astrocytoma WHO grade III ($n = 7$), B-cell lymphoma ($n = 4$), malignant oligodendroglioma WHO grade III ($n = 3$), and IgA-producing plasmocytoma ($n = 1$). The diagnoses of low-grade tumors were astrocytoma WHO grade II ($n = 3$), infiltrating astrocytoma grade II ($n = 1$), gangliogliomа ($n = 2$), and oligodendroglioma ($n = 2$). Thirty-three patients (mean age, 45.2 ± 11.5 years; 11 men) were diagnosed with nonneoplastic lesions. These lesions consisted of stroke ($n = 4$, no biopsies, and followed up for 4 months to 3 years with evidence of regression or expected evolution toward encephalomalacia); demyelinating disease ([$n = 10$, 1 biopsy], 5 cases of multiple sclerosis, 4 cases of acute disseminated encephalomyelitis [ADEM] followed up between 2 months and 3 years, and 1 case of progressive multifocal leukoencephalopathy with positive human polyoma virus in the CSF); benign lesions proved on clinical or pathologic examination ([$n = 10$, 4 biopsies], radionecrosis confirmed on surgical procedure [$n = 3$]; vasculitis confirmed on surgical procedure [$n = 1$]; nonpathologically confirmed postsurgical gliosis [$n = 2$] stable without evidence of recurrence for 2.5 and 8 years, hematoma [$n = 1$] demonstrating regression within 7 months, ataxia-telangiectasia [$n = 1$] with intracranial involvement, and chemotherapy-induced leukoencephalopathy [$n = 1$] stable for 3 years; and biologically proved meningoencephalitis [$n = 1$] that had improved at 1 month follow-up). Nine patients had stable lesions confirmed without pathologic examination that have been followed up for 11 months to 10 years with no evidence of progression and clinical deterioration. The local institutional review board approved the study.

We performed brain MR imaging and multisection ^{1}H-MRSI at 1.5T with Signa 5X and LX systems (GE Healthcare, Milwaukee, Wis) using a standard quadrature birdcage head coil. Routine brain MR imaging consisted of sagittal spin-echo (SE) T1-weighted images (TR, 300 ms; TE, 9 ms), axial fast SE (FSE) T2-weighted images with fat suppression (TR, 5800 ms; TE, 108 ms), axial fluid-attenuated inversion recovery (FLAIR) (TR, 8802 ms; TE, 133 ms; TI, 2200 ms), and axial and coronal T1-weighted SE images (TR, 500 ms; TE, 9 ms) after administration of contrast (gadolinium-diethylenetriamine pentaacetic acid [Gd-DTPA]) at 0.1 mmol/kg. Axial T1-weighted spoiled gradient-recalled localizer images (TR, 34 ms; TE, 5 ms) at the same section location and thickness as the proton MRSI scan were also obtained. We performed ^{1}H-MRSI using a multi-section spin-echo sequence (TE, 280 ms) with 2D circular phase-encoding, chemical shift selection water suppression, and outer-volume saturation pulses for lipid suppression.[15]

We adjusted the magnetic field homogeneity automatically, using the unsuppressed water signal intensity. Either three or four 15-mm-thick axial sections were obtained with an intersection gap of 2.5 mm. The axial MRSI sections were graphically prescribed from the sagittal T1-weighted images so that the center sections included the center of the lesion. However, in lesions in the temporal lobe, we positioned the sections so that the lowest section covered the main part of the lesion to avoid susceptibility artifacts. The TR was either 1700 ms (3 sections MRSI) or 2300 ms (4 sections MRSI). Because the T1 values of choline (Cho), creatine (Cr), and *N*-acetylaspartate (NAA) are similar, this small difference in TR between the 3- or 4-section scans has negligible influence on metabolite ratios. The scan time was either 22 or 30 minutes, depending on the TR used. The nominal voxel size was approximately 0.8 mL. In-plane nominal resolution was 7.5×7.5 mm^2. The multisection 2D MRSI datasets were processed by 3D Fourier transformation, with cosine filters in the spatial (phase-encoding) domains, and exponential line broadening of 3 Hz, zero-filling to 2048 data points, and a high-pass convolution filter to remove the residual water signal intensity (50 Hz stop-band) in the time-domain. No baseline correction was applied. We fitted the signals of Cho, Cr, NAA, and lactate to a Gaussian line shape using a simplex routine, and we performed reconstruction of the metabolite images by numeric integration. The peak area ratios of Cho/Cr, NAA/Cr, and NAA/Cho were calculated from the peak areas of the respective signals. Normalized lesion peak areas (Cho_{norm}, Cr_{norm}, and NAA_{norm}) expressed relative to the contralateral hemisphere were also calculated.

Regions of interest were selected in the lesion identified on MR imaging, and in contralateral hemisphere with normal MR imaging appearance. Care was taken to ensure that the region of interest was entirely within the solid part of the lesion (in the region showing the maximum abnormality—elevated Cho, and/or decreased NAA—as determined on the metabolite images) to avoid any contamination of the voxel from normal tissue, the area of necrosis, or cysts. In 2 cases, the lesion was located in the midline (1 demyelinating lesion in the genu of the corpus callosum and 1 lesion in the superior aspect of the cerebellar vermis); the control voxel was selected in a midline brain region with a normal MR imaging appearance (the splenium of the corpus callosum in the first case and the inferior aspect of the cerebellar vermis in the second case).

We performed dynamic susceptibility contrast-enhanced MR perfusion imaging in 32 patients (stroke, $n = 1$; demyelination, $n = 3$; stable lesion, $n = 8$; low-grade tumors, $n = 4$; and high-grade tumors, $n = 16$) using single-shot gradient-echo echo-planar imaging with 30 dynamic scans and a TR of 2 seconds and a TE of 60 ms. Seventeen sections were acquired with 5-mm section thickness/2.5-mm gap for a total of 510 images. The section locations were chosen to cover the lesion. We used a power injector to administer 0.1 mmol/kg of Gd-DTPA (Magnevist; Bayer HealthCare Pharmaceuticals, Wayne, NJ) at a rate of 5 mL/s into the antecubital vein through the catheter. The Gd-DTPA bolus was followed by a 20 mL saline flush at the same flow rate.

Tumors and nonneoplastic lesions: metabolite ratios and rCBV*

Metabolites	Low-Grade Tumors	High-Grade Tumors	All Tumors	Stroke	Demyelination	Proved Benign	Stable Lesions	All Nonneoplastic Lesions	P†
	N = 8	N = 28	N = 36	N = 4	N = 10	N = 10	N = 9	N = 33	
NAA/Cho	0.58 ± 0.31	0.34 ± 0.18	0.40 ± 0.23	0.72 ± 0.46	0.95 ± 0.39	1.08 ± 0.41	0.76 ± 0.22	0.91 ± 0.38	.0001
NAA/Cr	1.05 ± 0.51	0.78 ± 0.28	0.84 ± 0.36	1.02 ± 0.70	1.83 ± 1.01	1.06 ± 0.33	1.07 ± 0.40	1.29 ± 0.73	.002
Cho/Cr	2.10 ± 0.98	2.84 ± 2.43	2.68 ± 2.20	1.45 ± 0.55	1.88 ± 0.60	1.03 ± 0.23	1.40 ± 0.23	1.44 ± 0.52	.002
NAA_{norm}	0.43 ± 0.20	0.35 ± 0.15	0.37 ± 0.16	0.48 ± 0.36	0.64 ± 0.24	0.48 ± 0.17	0.53 ± 0.14	0.54 ± 0.21	.0001
Cho_{norm}	1.63 ± 0.44	2.10 ± 1.06	2.00 ± 0.98	1.05 ± 0.11	1.55 ± 0.56	0.75 ± 0.27	1.33 ± 0.31	1.19 ± 0.49	.0001
Cr_{norm}	0.94 ± 0.35	1.09 ± 0.52	1.06 ± 0.49	0.93 ± 0.25	1.02 ± 0.41	0.92 ± 0.37	1.06 ± 0.24	0.99 ± 0.33	NS
rCBV‡	1.45 ± 1.16	4.87 ± 3.12	4.11 ± 3.14	1.30	1.31 ± 0.49	0.77 ± 0.27	1.07 ± 0.44	1.00 ± 0.39	.002

Note:—NS indicates not significant; rCBV, relative cerebral blood volume; NAA/Cho, ratio of *N*-acetylaspartate to choline; NAA/Cr, ratio of *N*-acetylaspartate to creatine; Cho/Cr, ratio of choline to creatine.
* Data are presented as means ± standard deviations.
† *t* test comparison of tumors and nonneoplastic lesions.
‡ MRI perfusion cases: low-grade tumors (*N* = 4), high-grade tumors (*N* = 14), stroke (*N* = 1), demyelination (*N* = 2), proved benign (*N* = 5), stable lesions (*N* = 4).

We analyzed the MR perfusion data using in-house software (perfx; Johns Hopkins University School of Medicine, Baltimore, Md). Raw perfusion images were thresholded (typically 5% of maximum baseline image intensity) to remove noise pixels and were then converted to images of ΔR_2^* at each time point ($\Delta R_2^* = \ln[S/S_0]/TE$). The average of a range of preinjection images was used to calculate the S_0 image. The first pass of the bolus through the brain was then used to calculate indices of relative regional cerebral blood volume (rCBV) by integration of ΔR_2^*. After construction of rCBV maps, several measurements of regions of interest were obtained and expressed relative to the normal contralateral white matter, and we recorded the maximum rCBV.

We used unpaired *t* tests or analysis of variance with the Fisher Least Significant Difference post hoc test to evaluate the differences in metabolite ratios and rCBV between tumors and nonneoplastic lesions, and among the examined types of lesions. We applied discriminant function analysis to identify metabolite ratios that could predict inclusion in the biopsy-proved tumor group and nonneoplastic lesion group. We used an F test (Wilks lambda) to assess the significance of each discriminant function. Discriminant function analysis was also performed on the subset of patients who also had perfusion MR imaging, with rCBV as an additional parameter. In this subset of patients, we evaluated the discriminatory ability of MRSI, perfusion MR imaging, and a combination of the 2 approaches by constructing receiver operating characteristic (ROC) curves for each procedure. We compared the areas under the different curves with each other using the technique proposed by Hanley and McNeil.[16] A greater area under the curve indicates a better discriminatory ability of the corresponding imaging procedure. We also attempted to define cutoff points for MRSI and perfusion MR imaging for differentiating tumors from nonneoplastic lesions. We then calculated the accuracy (number of correct diagnoses/total number of subjects), sensitivity (number of correctly classified tumors/total number of tumor cases), specificity (number of correctly classified nonneoplastic lesions/total number of nonneoplastic lesions), positive predictive values (PPV, number of true tumor cases/all cases classified as tumors), and negative predictive values (NPV, number of true nonneoplastic cases/all cases classified as nonneoplastic lesions) associated with these cutoff points (all values are presented as %).

The level of statistical significance was set to $P < .05$. Data are presented as means ± standard deviations.

Results

The accompanying table shows average metabolite ratios and rCBV in tumors and nonneoplastic lesions. Examples of spectra, metabolite images, and CBV maps of a tumor and proved benign lesion are shown in Figs 1 and 2, respectively.

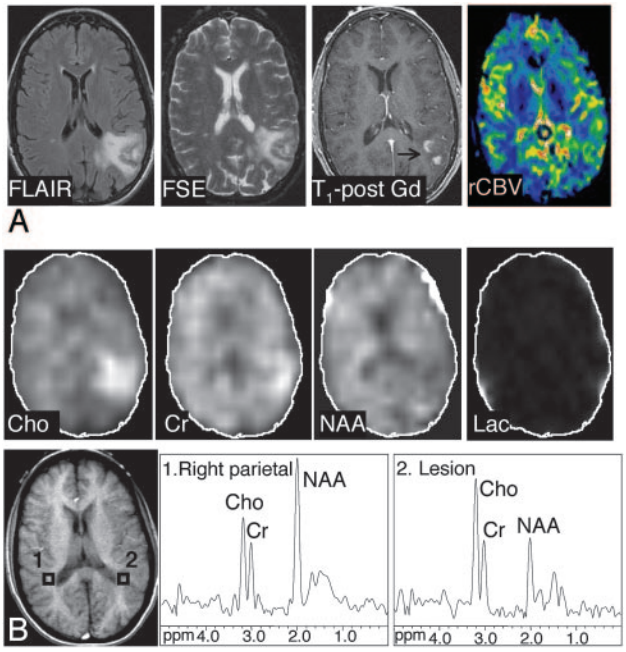

Fig 1. Axial FLAIR image, T2-weighted FSE MR image, axial contrast-enhanced T1-weighted SE MR image, and axial CBV map in a 38-year-old woman with primary CNS lymphoma. There is T2 hyperintensity involving the left temporoparietal lobe. There is minimal mass effect; the lesion exhibits patchy heterogeneous enhancement on the postgadolinium images. The CBV map demonstrates a moderately increased blood volume in the lesion compared with the normal contralateral side (rCBV, 1.66, which is higher than the cutoff point of 1.5). *A, B,* The abnormal signal intensity of the lesion extended over 8 FLAIR sections (5-mm section thickness, no gap; with 5 sections showing the bulk of the lesion). Images shown of the Cho, Cr, NAA, and lactate metabolites were reconstructed from the MRSI section exhibiting the largest metabolic abnormalities (MRSI, section 2). Axial T1-weighted SE localizer image with proton MR spectra of the lesion (voxel 2) and the corresponding control spectrum (voxel 1) are shown. Compared with the contralateral side, the metabolite images and spectra of the lesion show elevated Cho and Cr, and decreased NAA signals, with an NAA/Cho ratio of 0.58 (below the cutoff point of 0.61). Slight contamination of spectra with lipid signals, most likely because of the patient's head motion, was noted in this examination.

The NAA/Cho ratio was lower in high-grade tumors compared with demyelinating lesions (60.5%; $P < .001$), proved benign lesions (73.5%; $P < .0001$), stable lesions (41.0%; $P = .001$), stroke (37.2%; $P = .022$), and low-grade tumors (23.6%; $P = .051$). Low-grade tumors also had a lower NAA/Cho than the proved benign lesions (49.9%; $P = .001$) and demyelinating lesions (36.9%; $P = .011$). Both high-grade and

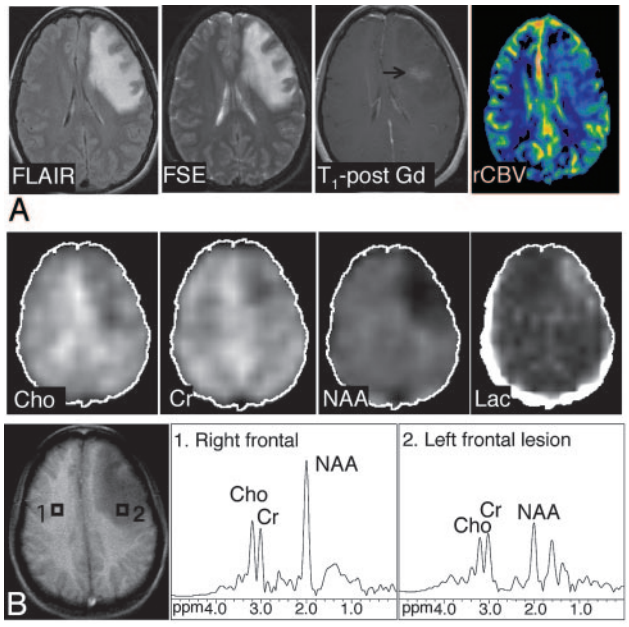

Fig 2. Axial FLAIR, T2-weighted FSE, contrast-enhanced T1-weighted SE MR images and axial CBV map in a 27-year-old woman with meningoencephalitis. There is an abnormal high T2 signal intensity in the left frontal lobe with minimal enhancement on the postgadolinium image. The CBV map shows slightly elevated levels of blood volume in the lesion compared with the normal contralateral side, with a rCBV of 1.35. The original diagnosis on the basis of conventional MR imaging favored a neoplasm over an inflammatory cause. At 3 weeks of follow-up (MR spectroscopy was not performed), an overall improved appearance with a decrease in the size of the frontal subcortical and deep white matter T2 signal intensity abnormality was noted. *A, B,* The abnormal signal intensity of the lesion extended over 5 FSE sections (5-mm section thickness, no gap; with 2 sections showing the bulk of the lesion). One MRSI section (the bottom section shown in the figure) covered the lesion. Images of the Cho, Cr, NAA, and lactate metabolites and proton MR spectra of the lesion (voxel 2) and control region (voxel 1) are shown. The NAA/Cho ratio of 1.15 was above the cutoff point of 0.61, Cho_{norm} was 0.8, and rCBV was slightly below the cutoff point of 1.5. On the basis of MRSI and perfusion MR imaging, the presence of a nonneoplastic lesion was favored. Discriminant function analysis classified this lesion as nonneoplastic on the basis of MRSI data alone and MRSI and perfusion MR imaging data.

low-grade tumors had a lower NAA/Cr ratio compared with demyelinating lesions (104.7%; $P < .0001$ and 77.4%; $P = .003$, respectively). High-grade tumors had a higher Cho/Cr ratio than the proved benign lesions (181.9%; $P = .004$) and stable lesions (144.2%; $P = .026$).

Cho_{norm} was higher in high-grade tumors compared with proved benign lesions (136.4%; $P < .0001$), stable lesions (77.6%; $P = .01$), stroke (105.8%; $P = .011$), and demyelinating lesions (56.1%; $P = .049$). Low-grade tumors had a 88.4% higher Cho_{norm} than the proved benign lesions ($P = .017$). High-grade tumors had a lower NAA_{norm} than demyelinating lesions (28.9%; $P < .0001$), stable lesions (17.5%; $P = .019$), and proved benign lesions (13%; $P = .067$), and low-grade tumors had a 21.3% lower NAA_{norm} than demyelinating lesions ($P = .021$). Cr_{norm} did not show any significant differences among the examined groups of lesions.

Considering all possible combinations of metabolite ratios, the best discriminant function to differentiate between the group of brain tumors (high-grade and low-grade) and the nonneoplastic lesions was found to include the ratios NAA/Cho, Cho_{norm}, NAA_{norm}, and NAA/Cr (presented in the decreasing magnitude of correlation with the discriminant function). The discriminant function analysis correctly classified 84.2% of original grouped cases in the tumor and nonneoplastic lesion groups ($P < .0001$). The discriminant function analysis misclassified 5 cases of tumors as nonneoplastic lesions (anaplastic astrocytoma WHO grade II, infiltrating astrocytoma WHO grade III, gliomatosis cerebri WHO grade II, oligodendroglioma WHO grade II, ganglioglioma WHO grade II). Six nonneoplastic lesions were classified as tumors: demyelination ($n = 1$), radiation necrosis ($n = 2$), postsurgical gliosis ($n = 1$), and stable lesions not confirmed on pathologic examination (1.5- to 2-year follow-up, $n = 2$).

We obtained good-quality perfusion data in 30 patients (Table); in 2 patients, perfusion MR imaging failed for technical reasons. High-grade tumors had a higher rCBV (4.9 ± 3.1; range, 1.2–11.3) than low-grade tumors (1.5 ± 1.2; range, 0.4–3.1; $P = .011$) and nonneoplastic lesions (1.0 ± 0.4; range, 0.5–0.7; $P < .001$). There were significant differences between the group of high-grade tumors and nonneoplastic lesions ($P = .001$), and between the high-grade and low-grade tumor groups ($P = .037$), whereas no significant difference was found between the low-grade tumor and nonneoplastic lesion groups ($P = .73$). In the 30 patients who were evaluated by MRSI and perfusion MR imaging, the discriminant function analysis correctly classified 93.3% of the original cases with the use of only spectroscopic data (the discriminant function contained NAA/Cho and NAA/Cr ratios; $P < .0001$), and 80% of original grouped cases were correctly classified with the use of the rCBV data only ($P = .002$).

Using discriminant function analysis, we found that perfusion MR imaging did not further improve the (already high) percentage of correctly classified cases using MRSI; 93.3% of the original grouped cases were correctly classified with use of combined spectroscopy and perfusion data (discriminant function included NAA/Cho, NAA/Cr and rCBV) ($P < .0001$). One case of a patient with a demyelinating lesion (rCBV = 1.66) was misclassified as a tumor, and 1 low-grade tumor (gliomatosis cerebri, rCBV = 3.1) was misclassified as a nonneoplastic lesion. In the analyses based on rCBV data only, 3 high-grade tumors (2 cases of anaplastic astrocytoma WHO grade III and 1 case of B-cell lymphoma) and 3 low-grade tumors (2 cases of oligodendroglioma WHO grade II and 1 case of ganglioglioma WHO grade I) were misclassified as nonneoplastic lesions. We carried out a further evaluation of discriminatory capability using the ROC analysis. The calculated areas under the ROC curves were 0.92 for MRSI, 0.89 for perfusion MR imaging, and 0.96 for the analysis with the use of MRSI and perfusion MR imaging (Fig 3). We found no significant differences when comparing the areas under the curves, which indicate that each procedure had a similar discriminatory capability.

In the daily practice of neuroradiology, it may be difficult to perform discriminant function analyses routinely. Therefore, we attempted to identify cutoff values, which could help differentiate tumors from nonneoplastic lesions. In our sample, it was not straightforward to find the optimum cutoff point for MRSI; the NAA/Cho range of 0.54 to 0.66 included 4 tumors (all NAA/Cho $\leq$0.61) and 5 nonneoplastic lesions (4 nonneoplastic lesions with NAA/Cho $>$0.61). With a cutoff value of NAA/Cho of 0.61 or less (corresponding to diagnosis of a tumor), accuracy was 84.1%, sensitivity 86.1%, specificity 81.8%, PPV 83.8%, and NPV 84.4% ($n = 69$ cases). All cases of patients with NAA/Cho of 0.61 or less had abnormally ele-

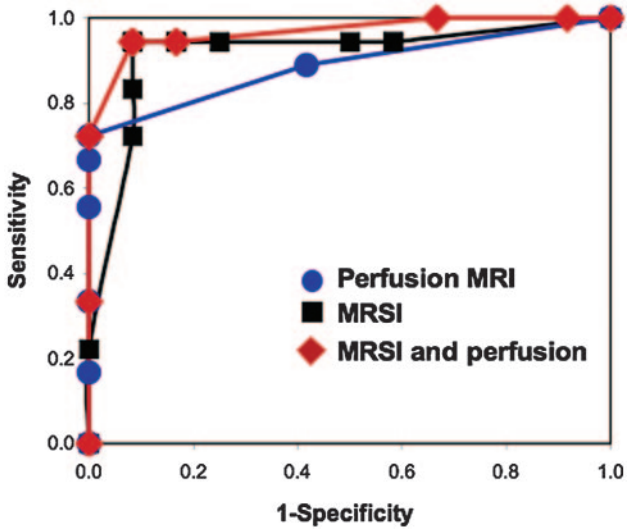

Fig 3. ROC curves representing discriminatory capability of perfusion MR imaging, ^{1}H-MRSI and combination of ^{1}H-MRSI and perfusion MR imaging to differentiate between tumors and nonneoplastic lesions. We constructed the curves using data on 30 subjects evaluated with both perfusion MR imaging and MRSI. The calculated areas under the ROC curves were 0.92 for MRSI, 0.89 for perfusion MR imaging, and 0.96 for the analysis on the basis of MRSI and perfusion MR imaging. We found no significant differences when comparing the areas under the curves, indicating that each procedure had similar discriminatory capability for these subjects.

vated Cho; however, there was an overlap in Cho_{norm} with nonneoplastic lesions (range, 0.38–2.32). Similar values were obtained for the subset of cases with perfusion MR imaging (n = 30): for NAA/Cho of 0.61 or less, accuracy was 86.7%, sensitivity 88.9%, specificity 83.3%, PPV 88.8%, and NPV 83.3%. For a simple decision making, NAA_{norm} and NAA/Cr were not of high diagnostic value because of a considerable overlap between tumors and nonneoplastic lesions for both parameters. A cutoff value of rCBV of 1.5 or more (corresponding to a diagnosis of a tumor) resulted in an accuracy of 83.3%, sensitivity 77.8%, specificity 91.7%, PPV 93.3%, and NPV 91.7%. With combined criteria (NAA/Cho $\leq$0.61 and rCBV $\geq$1.5), we obtained accuracy 80.0%, sensitivity 72.2%, specificity 91.7%, PPV 93.3%, and NPV 91.7%.

Discussion

The primary result of our study was a good specificity of ^{1}H-MRSI for distinguishing between high-grade and low-grade tumors, as well as between neoplastic lesions of all grades and benign lesions in adults. Perfusion MR imaging was also able to successfully distinguish high-grade and low-grade tumors, as well as high-grade tumors from benign lesions. However, no significant differences were found between low-grade tumors and benign lesions. Adding rCBV measurements did not improve the discriminant analysis classification of lesions with that on the basis of MRSI alone.

In our group of patients with heterogeneous brain lesions evaluated for suspected neoplasm, ^{1}H-MRSI and discriminant function analysis demonstrated a high rate of success of 84% in correctly classifying lesions originally diagnosed as tumors and nonneoplastic lesions on the basis of the ratios of NAA/Cho, Cho_{norm}, NAA_{norm}, and NAA/Cr. As expected, elevated levels of Cho were detected in tumors compared with nonneoplastic lesions. Elevated signal intensity in Cho results from increased attenuation of proliferating tumoral cells, with Cho-containing compounds including membrane precursors and products of degradation. Tumoral levels of NAA, presumably originating from residual brain tissue within an infiltrating tumor,[17,18] were lower than in nonneoplastic lesions. Thus, in agreement with published data, our analyses confirmed that highly elevated Cho-containing compounds in conjunction with a decreased NAA resonance (resulting in decreased ratio of NAA/Cho) are parameters sensitively indicative of neoplastic tumoral growth[19,20] and are helpful in differentiating tumors from other causes. There was no significant difference in the level of Cr among the groups of different lesions. The levels of Cr in tumors in adults have been reported to be decreased[18] or both increased and decreased.[21] In our study, high-grade tumors had a wider range of levels of Cr than low-grade tumors. The lowest Cr levels (28% of the control value) were found in a B-cell lymphoma, whereas the largest Cr_{norm} (2.63) was detected in the case of a patient with anaplastic astrocytoma (Cr_{norm} in anaplastic astrocytomas were variable, 1.36 $\pm$ 0.72 on average). Two cases of patients with anaplastic astrocytoma from a previously examined pediatric group[14] also had relatively high Cr_{norm} (1.27 and 1.40) compared with other high-grade tumors. The presence of elevated lactate was confirmed only in 2 cases of high-grade tumors (1 glioblastoma multiforme and 1 anaplastic astrocytoma) and 1 case of a stroke. In the remaining tumors, lactate was either not detected or, in some cases, was obscured because of contamination by the lipid peaks from the skull and scalp. Because the voxels selected for evaluations were from the solid part (often the rim) of the tumor, lactate from areas of necrosis was avoided.

In our study, in some instances, tumors of grades II and III were misclassified as benign lesions, and some cases of demyelination, radiation necrosis, gliosis, and stable lesions were misclassified as tumors. Misclassification of tumors as benign lesions can occur either as a result of high tumoral heterogeneity, when regions of spectroscopic sampling differ from the location of the highest tumor grade on histologic examination (which presumably exhibit the highest levels of Cho), or in tumors showing no increase in Cho.[22,23] In agreement with these findings, the 5 misclassified tumors had the highest NAA/Cho ratio ($\geq$0.7) of all tumors. This result is similar to a previous study (including 86 cases of tumors and 13 nonneoplastic lesions) showing a NAA/Cho ratio of less than 1 as a threshold value for tumors.[6]

The diagnosis of demyelinating lesions, multiple sclerosis, and ADEM is made on typical clinical presentation, conventional MR imaging findings, and the evolution and presentation of the disease with time. However, on occasion demyelinating disease presents as a single brain mass that is indistinguishable from a brain tumor on clinical and radiologic examinations. In those cases, ^{1}H-MRSI has an important diagnostic role, especially when it reveals reduced NAA without increased Cho. In these instances, MR spectroscopic findings may help spare the patient from brain biopsy. Nonetheless, some cases of active demyelinating lesions may show similar spectra as high-grade gliomas (ie, decreased NAA and highly elevated Cho),[24] because of histopathologic similarities, which include hypercellularity, reactive astrocytes, mitotic figures, and areas of necrosis. In our study, the misclassified case

of demyelination had the lowest NAA/Cho ratio (0.24) of all demyelinating lesions. The lesion also showed increased rCBV on the perfusion scan.

Differentiating residual or recurrent tumor from treatment-related changes is limited on conventional MR imaging as well as on histologic examination; areas of T1 contrast enhancement after radiation treatment often contain both residual or recurrent tumor and tissue affected by therapy-related changes. Besides that, the heterogeneity of gliomas before and after therapy and the inaccuracy of biopsy sampling pose another challenge in the histologic separation of tumors from necrosis.[25] Low levels of Cho and Cr can differentiate radiation necrosis from recurrent or progressive tumors.[26,27] In our study, 2 of 3 cases of radiation necrosis were misclassified as tumors; this could be related to an increase in Cho-containing compounds after radiation therapy as a result of cell damage and astrogliosis. In addition, both tumors and necrotic tissue have low levels of NAA, consistent with neuronal damage that is present in tumors as well as in radiation necrosis. However, the misclassification of the 2 cases of radiation necrosis as tumors was somewhat surprising, given their high NAA/Cho ratio (1.35 and 1.65; in all tumors, NAA/Cho was $\leq$0.99) and decreased Cho_{norm} (0.63 and 0.58; all tumors had Cho_{norm} $\geq$1.04). However, in the subgroup of patients evaluated by MRSI and perfusion MR imaging, one of these cases was classified correctly as a nonneoplastic lesion (perfusion MR imaging showed decreased rCBV).

Perfusion MR imaging provides measurement of tumoral angiogenesis and capillary permeability, which may aid in the diagnosis, grading, and prognosis of gliomas. Primary high-grade neoplasms and metastases are expected to have elevated rCBV because of intensive neoangiogenesis and high metabolism, whereas rCBV is typically lower or normal in low-grade neoplasms and nonneoplastic lesions.[13] Law et al[28] suggested a cutoff value of 1.75 for rCBV for diagnosis of high-grade gliomas. However, rCBV was also found to vary among different types of low-grade tumors (eg, oligodendrogliomas have been reported to have higher rCBV than astrocytomas).[29] Although oligodendrogliomas tend to be high-blood volume tumors, with a wide range of rCBV values,[29,30] some low-grade oligodendrogliomas may not show increased rCBV.[30] In agreement with these findings, 1 case of nonanaplastic oligodendroglioma in our study showed a decreased rCBV of 0.4, and 1 case of anaplastic oligodendroglioma showed a rCBV of 2.5. In our study, the rCBV of low-grade tumors varied between 0.40 and 3.07, and the range of rCBV in high-grade tumors was 1.22 to 10.34. Perfusion MR imaging can also help differentiate between recurrent tumors and radiation necrosis; recurrent tumors have a higher rCBV compared with radiation necrosis.[31,32] Perfusion MR imaging has been shown to be a valuable diagnostic tool in distinguishing active demyelinating lesions from brain tumors, on the basis of elevated rCBV in tumors.[33] In a subgroup of subjects with both MRSI and perfusion MR imaging examinations, the diagnostic accuracy (compared with discriminant function analysis) of MRSI was higher than perfusion MR imaging alone, and the combination of MRSI and perfusion MR imaging did not further improve the overall diagnostic accuracy of MRSI. This finding was mainly the result of overlap in rCBV between the group of stable lesions (rCBV, 0.53–1.22) and low-grade tumors (rCBV, 0.40–3.07) and likely also because of a smaller number of cases of perfusion compared with the number of patients evaluated by MRSI. However, the ROC analysis, which has been very useful in radiologic decision making, did not find any difference in discriminatory capability between MRSI and perfusion MR imaging.

There were several limitations of our study. One potential limitation was that the rCBV was evaluated in regions corresponding to those with the most abnormal MR spectra. Although Cho and NAA are considered measures of cellular proliferation, and neuronal viability, respectively, rCBV may reflect endothelial proliferation and angiogenesis. Because these biologic entities are different from a pathologic standpoint, it may be possible that in some lesions, the largest abnormalities may be found in different spatial locations within the lesion. We found this to be the case in 1 glioblastoma multiforme and 1 anaplastic astrocytoma, in which a higher rCBV was detected in a section adjacent to the section included for analysis. Because both types of tumors had a highly elevated rCBV throughout the lesion, selection of a different region of interest for evaluation did not affect our results.

Another potential limitation was that biopsies were not available for all cases included in the group of nonneoplastic lesions. Therefore, it may be possible that some of the lesions (including 2 stable lesions misclassified by the discriminant analysis as tumors) may have been low-grade tumors. However, excluding stable and gliotic lesions from the discriminant function analysis did not improve the classification. In our study, we made no attempt to compare MRSI or perfusion classification with diagnoses on the basis of conventional MR imaging and clinical information, so we could not assess the added value of these techniques. Also, we did not analyze other parameters that may have been extracted from perfusion MR imaging time curves, such as vascular permeability. Another potential limitation was that MRSI was performed at long TE for technical reasons (it is difficult to perform MRSI at short TE with extensive brain coverage, mainly because of inhomogeneities in the B0 magnetic field). For this reason, compounds such as glutamate, glutamine, myo-inositol, or lipids could not be evaluated in our study. It is possible that future studies of MRSI at short TE that observe these compounds may improve the performance of MRSI further in distinguishing benign from malignant brain lesions.

In contrast to several previous studies, our study used high-resolution multisection ^{1}H-MRSI, which allowed the selection of a voxel with the most abnormal spectroscopic appearance in heterogeneous lesions. It also automatically provided control spectra from the normal-appearing contralateral hemisphere. Both of these factors may have helped improve diagnostic accuracy; in a previous study, a normalized Cho ratio was found to be a better measurement than either the Cho/Cr or Cho/NAA ratios,[34] because the normalized value controls for the intersubject differences in metabolite levels. We used metabolite ratios to control for the potential presence of CSF, cystic fluid, or necrosis (though we tried to avoid these regions in the analyses) in the spectroscopic voxel. Partial volume effects of CSF with the normal brain was also minimized by the high spatial resolution of this technique (nominal voxel size, 0.8 mL), which is much better than that commonly used in

single-voxel spectroscopy (typically, 8 mL).[1] Although our study used ^{1}H-MRSI at long TE, which results in lower signal-to-noise ratios compared with short TE acquisitions, it provides less complex spectra that are more simple to analyze because of the flat baseline, lack of spectral overlap, and attenuation of water and lipid signals resulting from T2 relaxation.

In summary, the results of this study show that ^{1}H-MRSI may be helpful in the assessment of undiagnosed brain lesions. In particular, ^{1}H-MRSI differentiated the group of low-grade tumors, in which it demonstrated elevated Cho and decreased NAA from nonneoplastic lesions. Perfusion MR imaging and the combination of ^{1}H-MRSI and perfusion MR imaging were found to have comparable ability to ^{1}H-MRSI alone in differentiating tumors from nonneoplastic lesions. In the future, technical advances in ^{1}H-MRSI, including the use of higher magnetic field strengths, may further improve diagnostic accuracy because of higher spectral resolution and increased signal-to-noise ratios. In the long term, it is hoped that improvements in the diagnosis of lesions with ^{1}H-MRSI and perfusion MR imaging will reduce the need for brain biopsy, especially in cases of inaccessible lesions or lesions located in crucial brain structures (eg, brain stem or eloquent cortex).

Acknowledgments

We thank Ms. Priscilla Matthews for her help with editing the manuscript.

References

1. Rand SD, Prost R, Haughton V, et al. **Accuracy of single-voxel proton MR spectroscopy in distinguishing neoplastic from nonneoplastic brain lesions**. *AJNR Am J Neuroradiol* 1997;18:1695–704
2. Burger PC. **Malignant astrocytic neoplasms: classification, pathologic anatomy, and response to treatment**. *Semin Oncol* 1986;13:16–26
3. Al-Okaili RN, Krejza J, Woo JH, et al. **Intraaxial brain masses: MR imaging-based diagnostic strategy—initial experience**. *Radiology* 2007;243:539–50
4. Poptani H, Gupta RK, Roy R, et al. **Characterization of intracranial mass lesions with in vivo proton MR spectroscopy**. *AJNR Am J Neuroradiol* 1995;16:1593–603
5. Poptani H, Kaartinen J, Gupta RK, et al. **Diagnostic assessment of brain tumours and non-neoplastic brain disorders in vivo using proton nuclear magnetic resonance spectroscopy and artificial neural networks**. *J Cancer Res Clin Oncol* 1999;125:343–49
6. Butzen J, Prost R, Chetty V, et al. **Discrimination between neoplastic and nonneoplastic brain lesions by use of proton MR spectroscopy: the limits of accuracy with a logistic regression model**. *AJNR Am J Neuroradiol* 2000;21:1213–19
7. Möller-Hartmann W, Herminghaus S, Krings T, et al. **Clinical application of proton magnetic resonance spectroscopy in the diagnosis of intracranial mass lesions**. *Neuroradiology* 2002;44:371–81
8. De Stefano N, Caramanos Z, Preul MC, et al. **In vivo differentiation of astrocytic brain tumors and isolated demyelinating lesions of the type seen in multiple sclerosis using 1H magnetic resonance spectroscopic imaging**. *Ann Neurol* 1998;44:273–78
9. Venkatesh SK, Gupta RK, Pal L, et al. **Spectroscopic increase in choline signal is a nonspecific marker for differentiation of infective/inflammatory from neoplastic lesions of the brain**. *J Magn Reson Imaging* 2001;14:8–15
10. Vuori K, Kankaanranta L, Häkkinen AM, et al. **Low-grade gliomas and focal cortical developmental malformations: differentiation with proton MR spectroscopy**. *Radiology* 2004;230:703–08
11. Pandya HG, Wilkinson ID, Agarwal SK, et al. **The nonspecific nature of proton spectroscopy in brain masses in children: a series of demyelinating lesions**. *Neuroradiology* 2005;47:955–59
12. Cha S, Knopp EA, Johnson G, et al. **Intracranial mass lesions: dynamic contrast-enhanced susceptibility-weighted echo-planar perfusion MR imaging**. *Radiology* 2002;223:11–29
13. Law M, Hamburger M, Johnson G, et al. **Differentiating surgical from nonsurgical lesions using perfusion MR imaging and proton MR spectroscopic imaging**. *Technol Cancer Res Treat* 2004;3:557–65
14. Hourani R, Horská A, Albayram S, et al. **Proton magnetic resonance spectroscopic imaging to differentiate between nonneoplastic lesions and brain tumors in children**. *J Magn Reson Imaging* 2006;23:99–107
15. Duyn JH, Gillen J, Sobering G, et al. **Multisection proton MR spectroscopic imaging of the brain**. *Radiology* 1993;188:277–82
16. Hanley JA, McNeil BJ. **A method of comparing the areas under receiver operating characteristic curves derived from the same cases**. *Radiology* 1983;148:839–43
17. Gill SS, Thomas DG, Van Bruggen N, et al. **Proton MR spectroscopy of intracranial tumours: in vivo and in vitro studies**. *J Comput Assist Tomogr* 1990;14:497–504
18. Howe FA, Barton SJ, Cudlip SA, et al. **Metabolic profiles of human brain tumors using quantitative in vivo 1H magnetic resonance spectroscopy**. *Magn Reson Med* 2003;49:223–32
19. Preul MC, Caramanos Z, Collins DL, et al. **Accurate, noninvasive diagnosis of human brain tumors by using proton magnetic resonance spectroscopy**. *Nat Med* 1996;2:323–25
20. Burtscher IM, Skagerberg G, Geijer B, et al. **Proton MR spectroscopy and preoperative diagnostic accuracy: an evaluation of intracranial mass lesions characterized by stereotactic biopsy findings**. *AJNR Am J Neuroradiol* 2000;21:84–93
21. Nelson SJ. **Multivoxel magnetic resonance spectroscopy of brain tumors**. *Mol Cancer Ther* 2003;2:497–507
22. Saraf-Lavi E, Bowen BC, Pattany PM, et al. **Proton MR spectroscopy of gliomatosis cerebri: case report of elevated myoinositol with normal choline levels**. *AJNR Am J Neuroradiol* 2003;24:946–51
23. Londoño A, Castillo M, Armao D, et al. **Unusual MR spectroscopic imaging pattern of an astrocytoma: lack of elevated choline and high myo-inositol and glycine levels**. *AJNR Am J Neuroradiol* 2003;24:942–45
24. Saindane AM, Cha S, Law M, et al. **Proton MR spectroscopy of tumefactive demyelinating lesions**. *AJNR Am J Neuroradiol* 2002;23:1378–86
25. Cha S. **Update on brain tumor imaging: from anatomy to physiology**. *AJNR Am J Neuroradiol* 2006;27:475–87
26. Taylor JS, Langston JW, Reddick WE, et al. **Clinical value of proton magnetic resonance spectroscopy for differentiating recurrent or residual brain tumor from delayed cerebral necrosis**. *Int J Radiat Oncol Biol Phys* 1996;36:1251–61
27. Rock JP, Hearshen D, Scarpace L, et al. **Correlations between magnetic resonance spectroscopy and image-guided histopathology, with special attention to radiation necrosis**. *Neurosurgery* 2002;51:912–19; discussion 919–20
28. Law M, Yang S, Wang H, et al. **Glioma grading: sensitivity, specificity, and predictive values of perfusion MR imaging and proton MR spectroscopic imaging compared with conventional MR imaging**. *AJNR Am J Neuroradiol* 2003;24:1989–98
29. Cha S, Tihan T, Crawford F, et al. **Differentiation of low-grade oligodendrogliomas from low-grade astrocytomas by using quantitative blood-volume measurements derived from dynamic susceptibility contrast-enhanced MR imaging**. *AJNR Am J Neuroradiol* 2005;26:266–73
30. Lev MH, Ozsunar Y, Henson JW, et al. **Glial tumor grading and outcome prediction using dynamic spin-echo MR susceptibility mapping compared with conventional contrast-enhanced MR: confounding effect of elevated rCBV of oligodendrogliomas [corrected]** [published erratum appears in *AJNR Am J Neuroradiol* 2004;25:B1]. *AJNR Am J Neuroradiol* 2004;25:214–21
31. Covarrubias DJ, Rosen BR, Lev MH. **Dynamic magnetic resonance perfusion imaging of brain tumors**. *Oncologist* 2004;9:528–37
32. Sugahara T, Korogi Y, Tomiguchi S, et al. **Posttherapeutic intraaxial brain tumor: the value of perfusion-sensitive contrast-enhanced MR imaging for differentiating tumor recurrence from nonneoplastic contrast-enhancing tissue**. *AJNR Am J Neuroradiol* 2000;21:901–09
33. Cha S, Pierce S, Knopp EA, et al. **Dynamic contrast-enhanced T2*-weighted MR imaging of tumefactive demyelinating lesions**. *AJNR Am J Neuroradiol* 2001;22:1109–16
34. Rabinov JD, Lee PL, Barker FG, et al. **In vivo 3-T MR spectroscopy in the distinction of recurrent glioma versus radiation effects: initial experience**. *Radiology* 2002;225:871–79